Anomalous behavior of higher-harmonic spin density waves in Mn_3Si

S. Tomiyoshi,[1] E. R. Cowley,[2] and H. Onodera[3]
[1]*Department of Materials Science and Engineering, Ehime University, Matsuyama 790-8577, Japan*
[2]*Rutgers University Camden College of Arts and Science, Camden, New Jersey 08102, USA*
[3]*Department of Physics, Tohoku University, Sendai 980-8575, Japan*
(Received 3 April 2005; revised manuscript received 28 October 2005; published 24 January 2006)

Higher-harmonic spin density waves (SDW's) in Mn_3Si have been investigated by neutron diffraction, and the third-harmonic satellites have been found to exist at low temperatures at the 3**Q** positions expected from the propagation wave vector **Q** of the fundamental satellite. The magnitude of the magnetic moments of the third harmonics is about 1/40 that of the fundamental. The third-harmonic satellites did not follow the usual temperature variation of a magnetization curve, but disappeared abruptly above 9 K. This is far below the Néel temperature of 23 K, and the temperature dependence suggests a first-order-type phase transition. Associated with this transition the intensity of the fundamental satellites changed slightly and the presence of the third harmonics suppressed the amplitude of the fundamental SDW. This transition was confirmed by specific heat measurements showing a small hump at 8.5 K, which persists to high magnetic fields of more than 6 T. The possibility of the presence of second-harmonic satellites is suggested, but it is not as clear as that of third-harmonic satellites in the present experiment. The existence of the third-harmonic satellites suggests that a transverse sinusoidal structure with spins modulating in the (110) or (210) plane is the most probable spin structure of Mn_3Si.

DOI: 10.1103/PhysRevB.73.024416 PACS number(s): 75.30.Fv

I. INTRODUCTION

In itinerant electron systems incommensurate spin structures occur due to spin density waves (SDW's). Chromium is known as a typical example of a material with incommensurate SDW's in 3*d* electron systems. It shows a long-period sinusoidal modulated spin structure with a propagation wave vector **Q** along the [100] direction, in which the SDW state is considered to occur due to the nesting between two pieces of Fermi surfaces separated by the wave vector **Q**.[1] The SDW due to the nesting mechanism occurs not only in metallic systems like chromium, but also in strong electron-electron-correlated systems such as high-T_c cuprates, where SDW instability is responsible for the anomalous normal-state transport property,[2] and in metal-insulator transition systems like $V_{2-x}O_3$.[3] Widespread application of this concept to the itinerant electron systems has led to a renewal of the study of the SDW state as well as careful study of metallic systems other than chromium, and Mn_3Si, which is a 3*d* electron system with more complex SDW states, is a very attractive target to be investigated more carefully.

Mn_3Si is an intermetallic compound with a cubic crystal structure of the DO_3 type (space group $Fm3m$) with a lattice constant of $a=5.722$ Å.[4] This is also an Heusler-type structure of the formula $Mn_{II2}Mn_ISi$ which can be described in terms of four fcc sublattices located at (0,0,0) for Mn_I, (1/4,1/4,1/4) and (3/4,3/4,3/4) for Mn_{II}, and (1/2,1/2,1/2) for Si as shown in Fig. 1. The Mn_I sites with an O_h point symmetry are surrounded by eight Mn_{II} nearest neighbors (NN's) and the Mn_{II} sites are, on the other hand, surrounded by four Mn_I NN's and four Si NN's, respectively. Due to their different nearest-neighbor configurations, Mn_I and Mn_{II} have different magnetic moments. This structure can be seen as a layered structure of (111) planes stacking along the [111] direction in a sequence of planes of Mn_I, Mn_{II}, and Si atoms, respectively, as shown in Fig. 1.

Mn_3Si becomes antiferromagnetic below the Néel temperature of $T_N=23$ K with the incommensurate spin structure of a propagation vector $\mathbf{Q}=0.425\mathbf{G}_{111}$, where $\mathbf{G}_{111}$ is a reciprocal lattice vector along the [111] direction [$\mathbf{G}_{111}=a^*(1,1,1)$, $a^*=2\pi/a$].[5,6] In this structure the deviation from commensurability, $\delta=(1/2)\mathbf{G}_{111}-0.425\mathbf{G}_{111}=0.075\mathbf{G}_{111}$, is small, so the magnetic satellite peaks appear near the commensurate antiferromagnetic point $(1/2)\mathbf{G}_{111}$ across the first Brillouin zone boundary in pairs along the $\langle 111\rangle$ direction as shown in Fig. 2, where the position of the fundamental satellites is shown as a grey square in the $(1\bar{1}0)$

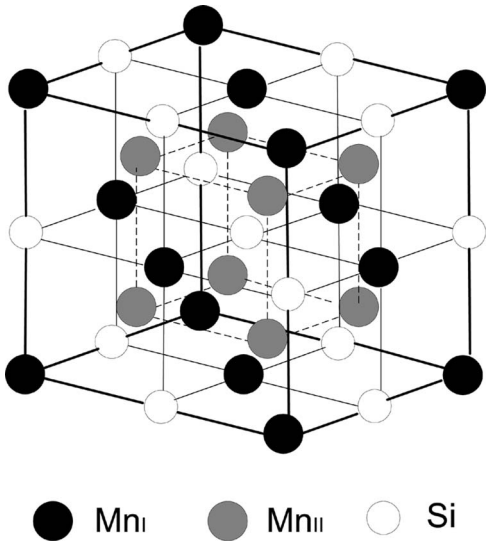

FIG. 1. Crystal structure of Mn_3Si. The layers of Mn_I, Mn_{II}, and Si stack along the [111] direction.

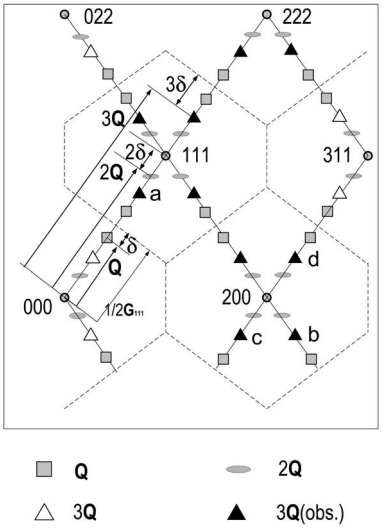

FIG. 2. The $(1\bar{1}0)$ reciprocal plane of Mn_3Si. Satellite positions of the 1**Q**, 2**Q**, and 3**Q** harmonics are shown as squares, ellipsoids, and triangles, respectively. Dotted lines show first Brillouin zone boundary. *a*, *b*, and *c* in the figure show 3**Q** satellites peaks shown in Fig. 3.

reciprocal lattice plane. Also, in Fig. 2, the expected positions of the second- and third-harmonic satellites are displayed as an ellipsoid and a triangle, respectively, for directions of the wave vector along [111] and $[\bar{1}11]$. In addition, the boundaries of the first Brillouin zone with a hexagon shape centered at the fcc-type reciprocal lattice points are shown as dotted lines.

From the analysis of neutron diffraction data the spin structure has been determined to be either a helical or a transversal sinusoidal structure. Which structure is correct has not yet been determined because of the difficulty in determining the incommensurate spin structure by unpolarized neutron diffraction for a cubic crystal with the multi-**Q** domain distribution.[6] The magnetic moments of MnI and MnII determined from the analysis of fundamental satellites by assuming a helical structure are $1.7\mu_B$ and $0.2\mu_B$, respectively, but for a transversal sinusoidal structure the maximum amplitudes of their magnetic moment values are $2.4\mu_B$ and $0.28\mu_B$, respectively, a factor of $\sqrt{2}$ times larger than that of the former.[6] When the temperature is raised from low temperature the propagation vector **Q** keeps almost a constant value at low temperature and then increases gradually, and near T_N it approaches rapidly to the commensurate value of $(1/2)\mathbf{G}_{111}$.[6] This behavior is very similar to that of chromium.[7]

Because of the small magnetic moments and low T_N, Mn_3Si is considered to be a weak magnetic material whose magnetic properties may show strong sensitivity to high magnetic fields. However, in Mn_3Si the magnetic susceptibility, specific heat and electrical resistivity keep their stiffness against magnetic fields up to 14 T (Refs. 8 and 9) and the magnetization does not show a saturation even in strong magnetic fields up to 50 T (Ref. 10). In Mn_3Si these tiny responses to high magnetic fields are considered to be due to the half metallic behavior that is peculiar to Heusler-type compounds.[11]

Inelastic neutron scattering experiments on Mn_3Si also revealed excitation spectra that were unusual in a number of ways. Below T_N, antiferromagnetic spin waves with a low velocity of $c=37$ meV Å emanate from the respective satellite positions, but above an energy of 6 meV $(3k_BT_N)$ the excitations become broadened, persisting to very high energy around the magnetic Brillouin zone center,[12,13] which perhaps should not be interpreted as propagating spin waves. These behaviors are not consistent with the usual Fermi-liquid concept[9,10] and have attracted interest in recent years. The magnetic properties of Mn_3Si described above have many similarities to those of the SDW's of chromium and to investigate problems pertinent to the SDW's will give useful information about itinerant electron states in 3*d* systems.

As is well known, the most characteristic features of the SDW's in chromium are the higher harmonics which accompany them. Tsunoda *et al.*[14] observed first the second harmonics by x-ray diffraction, and subsequently second and third harmonics have been observed by neutron diffraction by Pynn *et al.*[15] Recently more accurate studies have been performed by x-ray diffraction and the existence of the fourth-order harmonics has been identified.[16]

According to Hirai,[17] in itinerant electron systems a sinusoidal SDW deforms from a pure sine wave in general and higher harmonic SDW occurs, which can be expressed as a Fourier series

$$\mu_i = M_1 \cos(\mathbf{Q}\cdot\mathbf{R}_i) + M_3 \cos(3\mathbf{Q}\cdot\mathbf{R}_i) + M_5 \cos(5\mathbf{Q}\cdot\mathbf{R}_i) + \cdots, \quad (1)$$

where the magnitude of local moment μ_i at the *i*th site $(\mathbf{R}_i)$ is defined by $\mu_i = n_{i\uparrow} - n_{i\downarrow}$, $n_{i\uparrow}$, $n_{i\downarrow}$ are electron densities with up and down spins, respectively, at site *i* in the muffin-tin sphere, and $M_1, M_3, M_5, \ldots$ are amplitudes of the magnetic moments of odd order. Due to the formation of higher-harmonic SDW's a modulation of charge density occurs, which can be expressed as a Fourier series with even order $N_2, N_4, \ldots$:

$$n_i = N_0 + N_2 \cos(2\mathbf{Q}\cdot\mathbf{R}_i) + N_4 \cos(4\mathbf{Q}\cdot\mathbf{R}_i) + \cdots, \quad (2)$$

where the charge density at site *i* is defined as $n_i = n_{i\uparrow} + n_{i\downarrow}$ and N_0 is average number of electrons in the muffin-tin sphere.

In the case of chromium the amplitude of the harmonics is approximately $M_3/M_1 = 1/60$ and N_2 gives neutron scattering intensity comparable to or more than that from M_3 for reflections near the origin of the reciprocal lattice.[15] For Mn_3Si it is also natural to consider that the SDW accompanies higher-harmonic satellites with amplitudes similar to that in chromium. In the present work we investigated higher-harmonic SDW's in Mn_3Si by neutron diffraction using a mult-**Q**-domain sample and found that third-order harmonic satellites exist below the Néel temperature. However, the satellites show an unusual temperature behavior, disappearing at a low temperature far below the Néel temperature. To confirm this transition measurements of the specific heat and magnetic susceptibility were also performed.

II. EXPERIMENT

A. Sample preparation

Single-crystal samples of Mn_3Si were obtained using a traveling solvent zone (TSZ) method following the procedures described below. First, two types of rods, one Mn rich and the other in stoichiometric concentrations, were prepared by melting in an alumina crucible evacuated in a silica tube, using 99.9%-purity Mn and 99.999%-purity Si as starting materials. A Mn-rich rod with a length comparable to the width of the melting zone was sandwiched by stoichiometric ones and set vertical in a high-frequency induction heating furnace filled with He gas at 30 atm. The melting started from the Mn-rich rod and was swept with a slow speed of 2 mm/h through the stoichiometric rods. In this process the Mn-rich part has a low melting temperature compared with that of the stoichiometric one, and as the melting zone shifts to the upper part the stoichiometric part begins to melt in by a diffusion process and Mn_3Si crystals with the stoichiometric composition condense into the bottom part. This method prevents the decomposition of Mn_3Si by a peritectic reaction into Mn_5Si_3 phase by keeping the temperature of the melting zone below 1070 °C.[18] By using this method we succeeded in getting a fairly high-quality single crystal with a volume of 1.5 cc and a mosaic width of 30 min. Also the contamination of the Mn_5Si_3 phase which orders antiferromagnetic below 68 K (Ref. 19) was kept to be a minimum; otherwise, its presence complicates the interpretation of data of neutron and magnetic measurements. The crystals thus obtained were used for the measurements of higher-harmonic satellites, magnetic susceptibility, and specific heat.

B. Measurements of higher-harmonic SDW's

For measurements of higher-harmonic SDW's a neutron triple-axis spectrometer at the Brookhaven High Flux Beam Reactor was used. To reduce the neutron background arising from inelastic scattering, an elastic mode of operation was employed by using a neutron analyzer reflecting from the (002) plane of pyrolytic graphite. A pyrolytic graphite filter was also used to remove the contamination of half-wavelength neutrons for both incident and scattered beams. The incident neutron wavelength is 2.36 Å. The sample used in the present measurement was a TSZ crystal cut to a volume of 1 cc and was sealed in an aluminum can filled with He gas and mounted in a helium cryostat with one of the [110] axes vertical to the scattering plane.

The third-order satellites (3**Q** harmonics) are expected to occur at positions of $G_{hkl}\pm 3\mathbf{Q}$, where G_{hkl} is a reciprocal lattice vector with fcc type indices hkl. For a wave vector $\mathbf{Q}=0.425a^*(111)$ a 3**Q** harmonic satellite $[3\mathbf{Q}=1.275a^*(111)]$ originating from the (000) nuclear point will appear in the next (111) zone across the zone boundary at (1.275 1.275 1.275) as shown in Fig. 2, where the expected positions of 3**Q** harmonics are shown as a triangle. For a **Q** vector propagating along the $[\bar{1}\bar{1}\bar{1}]$ direction a 3**Q** harmonic satellite originating from (222) is also expected to appear at (0.725 0.725 0.725). Further for a **Q** vector along the $\pm[\bar{1}11]$ directions 3**Q** harmonic satellites are expected in the (111) zone at positions of (0.725 1.275 1.275) and (1.275 0.725 0.725), and the same arrangement of the positions is repeated in the other Brillouin zone as shown in Fig. 2.

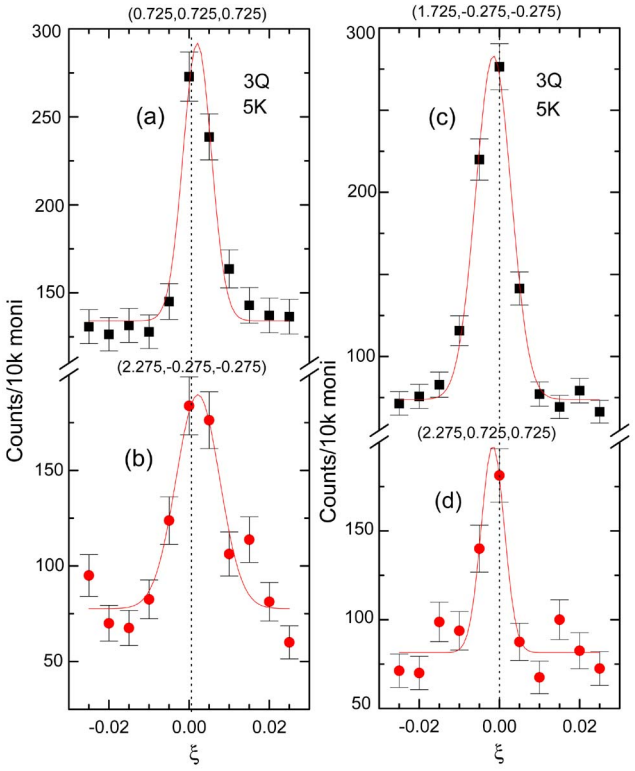

FIG. 3. (Color online) Four typical third-harmonic satellites (3**Q**) at 5 K as a function of a^*-axis coordinate ξ which is measured from the expected position for respective 3**Q** harmonics. The dotted lines show the expected 3**Q** positions at (a) (0.725,0.725,0.725), (b) (2.275,−0.275,−0.275), (c) (1.725,0.275,0.275), and (d) (2.275,0.725,0.725). The solid lines show Gaussian fitted curves. The triangle positions *a*, *b*, *c*, and *d* in Fig. 2 correspond to the peak positions of this figure.

We searched for the 3**Q** harmonic satellites in the (111) zone scanning along the [111] direction starting from (0.4 0.4 0.4) to (1.5 1.5 1.5) through (111) Bragg point at 5 K and found very small peaks at (0.725 0.725 0.725) and (1.275 1.275 1.275). We also found small peaks at (0.725 1.275 1.275) and (1.275 0.725 0.725) for a scan along the $[\bar{1}11]$ direction through the 111 nuclear peak. Similar scans were made in the (200) zones and we found peaks at the expected positions of the 3**Q** harmonic satellites shown in Fig. 2. The (222) zone is far from the origin, so due to the reduction of the magnetic form factor the intensity becomes weak; however, at the expected positions we could observe small peaks. All the 3**Q** harmonic satellites observed by the present experiment are shown as a black triangle (▲) in Fig. 2. Four typical peaks observed at 5 K are shown in Fig. 3 as a function of a^*-axis coordinate ξ, where $\xi=0$ means the expected position of 3**Q** harmonics, and the components of respective coordinates, for example, for peaks of Figs. 3(a) and 3(b) are $(0.725+\xi,0.725+\xi,0.725+\xi)$ and $(2.275+\xi,-0.275+\xi,-0.275+\xi)$, respectively. In Fig. 3 the intensity of neutron counts plotted is normalized to 10 k monitor counts for data

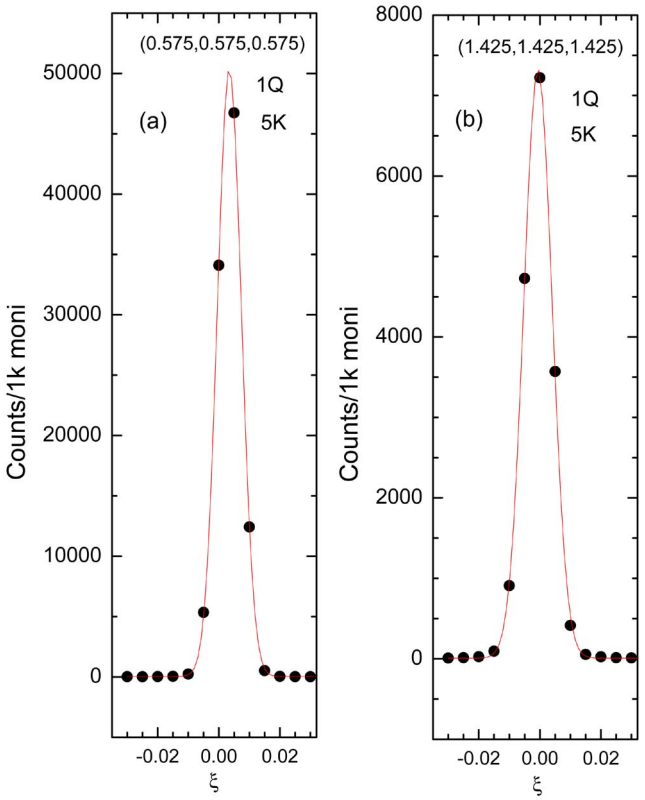

FIG. 4. (Color online) Two typical fundamental satellites (1**Q**) peaks at 5 K as a function of the a^*-axis coordinate ξ. Peak positions at (a) (0.575, 0.575, 0.575) and (b) (1.425, 1.425, 1.425). The solid lines show Gaussian-fitted curve.

measured with different counting times. As shown in the figure, the peak positions of all the peaks we could observe agree quite well with those of the expected positions (dotted line) within one step of the scan. That is the most important factor to make sure whether the observed peaks are due to 3**Q** harmonics or not. To check the peak positions more accurately an analysis by fitting the observed data using a Gaussian curve was carried out. The peak positions determined by the Gaussian fitting are within $\pm 0.005a^*$ for all the peaks observed in the (111) and (200) zones, and the agreement between observed and expected positions is excellent.

The next important step to verify that these arise from SDW order is to confirm that these peaks disappear in the paramagnetic state above the Néel temperature and all the peaks shown in Fig. 3 were found to disappear as the temperature was increased from 5 to 30 K. Some small peaks other than these were found to remain independent of the temperature above the T_N, but these spurious peaks were clearly separated from that of 3**Q** harmonic satellites.

To compare the intensity ratio of 3**Q** harmonics to that of the fundamental SDW's, 1**Q** peaks at (0.575 0.575 0.575) and (1.425 1.425 1.425) are shown in Fig. 4, where the neutron intensity is normalized to the monitor counts of 1k to make easy the comparison with those of 3**Q** harmonics shown in Fig. 3. The abscissa ξ means the a^*-axis coordinate measured from respective fundamental satellite positions mentioned above. The intensity ratio of 3**Q** to 1**Q** harmonics [compare Figs. 3(a) and 4(a)] is about 1/2500. In amplitude

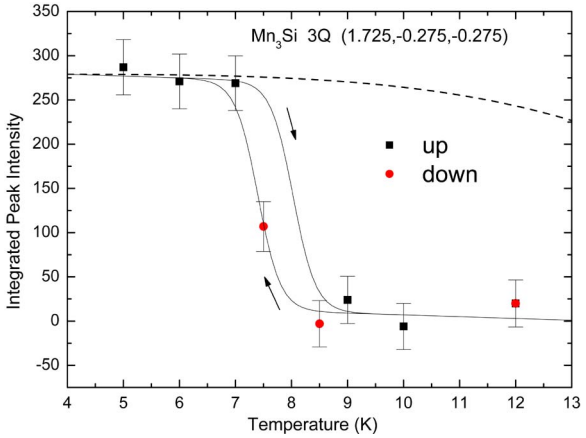

FIG. 5. (Color online) Integrated peak intensity of 3**Q** satellites at a position of (1.725, −0.275, −0.275) as a function of temperature for raising (■) and decreasing (●) temperatures. The solid lines show smoothing curves connecting data points, and the dotted line is the magnetization curve of a Brillouin curve with $S=1/2$.

ratio this is roughly equal to 1/50, of the same order observed in the 3**Q** harmonics in chromium. Next we compare the linewidth of the peaks between 3**Q** in Fig. 3 and fundamental satellites in Fig. 4. The full width at half maximum for both the 3**Q** harmonics and fundamental ones in Fig. 4 is about $0.01a^*$, though the full width varies a little depending on the geometrical configuration of the Bragg reflections (Lorentz factor). Therefore the magnetic reflections observed as 3**Q** harmonic satellites have similar coherent lengths with that of fundamental satellites. From the results mentioned above we can say that the observed peaks at positions $G_{hkl} \pm 3\mathbf{Q}$ in the (111) and (200) zones are 3**Q** harmonic satellites arising from SDW ordering in Mn_3Si.

The details of the temperature variation of 3**Q** harmonic satellites are surprising. The temperature dependence of the integrated intensity for a 3**Q** peak at (1.725 −0.275 −0.275), which has highest intensity observed in the present experiment, was measured from 5 to 12 K. The integrated intensity I_{3Q} (background counts subtracted) for the 3**Q** satellites is plotted for increasing (■) and decreasing (●) temperatures, respectively, in Fig. 5. As the temperature was increased, I_{3Q} decreased linearly at low temperatures, similar to the temperature variation of I_Q for a fundamental satellite shown as a dotted line, which is a Brillouin curve ($S=1/2$) normalized to $T_N=23$ K. Above 7 K, I_{3Q} decreased suddenly from the dotted line and dropped to zero above 9 K. I_{3Q} is expected to show a small decrease following a power law $I_{3Q}(T) \propto I_Q^3$ just below T_N as observed in chromium,[15] so this sudden drop is abnormal. The transition width in raising temperature is estimated to be within 1 K as shown in the figure as a solid line connecting data points. In decreasing temperature from 12 K, I_{3Q} began to increase below 8 K and rapidly returned to a saturated value below 6 K with a transition width of about 1 K. Evidently these heating and cooling processes show temperature hysteresis with a width of about 0.6 K. The sharp transition and hysteresis phenomena of 3**Q** harmonic satellites suggest that this is a first-order phase transition. In chromium the transition from the antiferroma-

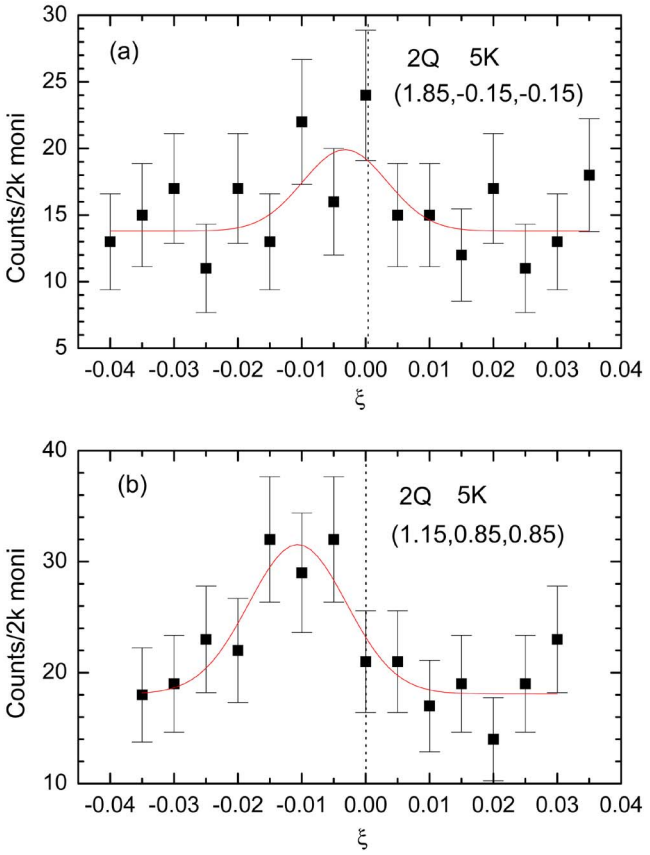

FIG. 6. (Color online) Scans at 5 K around 2**Q** harmonic satellites through positions of (a) $(1.85,-0.15,-0.15)$ and (b) (1.15,0.85,0.85) as a function of the a^*-axis coordinate ξ. The solid lines show Gaussian-fitted curve and the dotted lines show the expected position of the 2**Q** harmonic satellites. These 2**Q** peaks have a little weak intensity compared to 3**Q** harmonic satellites.

negetic to paramagnetic state is recognized as a first-order phase transition, where the fundamental and all the higher-harmonic satellites disappear together at the Néel temperature and no temperature hysteresis has been observed.[7] On the other hand, in Mn_3Si the fundamental satellites follow a second-order phase transition, but 3**Q** harmonics change following a first-order phase transition. Why such a difference occurs is a very interesting problem.

Next we describe our results for the second-order harmonics which arise from the charge density wave (CDW) and the strain wave due to the formation of SDW's as described by Eq. (2) in the Introduction. The peaks are expected to appear at $G_{hkl}\pm 2\mathbf{Q}$ i.e., $G_{hkl}\pm 0.15\mathbf{G}_{111}$, which is near the reciprocal lattice points as shown in Fig. 2, where an ellipsoid indicates the positions of second-order harmonics. The neutron scattering intensity due to the strain wave is proportional to $(\mathbf{q}\cdot\boldsymbol{\Delta})^2$, where $\mathbf{q}$ is the scattering vector and $\boldsymbol{\Delta}$ is the amplitude of the lattice distortion along the $\mathbf{Q}$ direction, so high scattering angles are favorable for the observation of second-order harmonics.[16] In a scan in the (200) zone a small peak was found at a 2**Q** position of $(1.85\ -0.15\ -0.15)$ as shown in Fig. 6(a). In this case the peak position agrees with that expected for 2**Q** harmonics. However, its identification is not certain because of poor counting statistics. To make clear the occurrence of this peak Gaussian fitting was applied and the curve fitting was found to converge easily. The following Gaussian parameters were obtained: peak center at a^* $(1.847,-0.153,-0.153)$ with an error of $\pm 0.004a^*$ and full width at half maximum (FWHM)$=0.014a^*\pm 0.008a^*$. This position parameter agrees quite well with that expected for 2**Q** harmonics, and the FWHM is in the range obtained for the Gaussian fitting applied to the Bragg reflections of fundamental and 3**Q** harmonic satellites observed in the present experiment. So this scan suggests possibility of 2**Q** harmonic satellites. And in a scan at (1.15, 0.85, 0.85) we observed a small peak as shown in Fig. 6(b), where by a Gaussian fitting the parameter obtained for full width at half maximum, FWHM$=0.015a^*\pm 0.006a^*$, is reasonable for a Bragg reflection, but the center of the peak shifts $0.01a^*$ away from the expected coordinate. This deviation is the largest in the present experiment, but it seems to be within the limit of experimental error. For other scans we could not find peaking at 2**Q** positions, probably due to poor counting statistics. For the two scans shown in Fig. 6 we did not perform a temperature variation measurement and the disappearance of these peaks above T_N has not been confirmed. Therefore in the present experiment we can point out only a possibility of occurrence of 2**Q** harmonic satellites. Perhaps with better counting statistics we would be able to observe second-order harmonic satellites at the all positions.

C. Measurement of fundamental SDW

In addition to the observation of 3**Q** harmonics and their anomalous temperature variation we performed measurements of fundamental satellites with the emphasis on their temperature dependence. The fundamental SDW satellites were measured using a two-axis neutron diffractometer, KSD, installed in a guide hall of the JRR-3M reactor at JAERI in Tokai, with an incident neutron beam of a wavelength of 1.527 Å, monochromated by the (111) plane of Ge crystals. The single-crystal sample used for the fundamental satellite measurements was the same one used for the higher-harmonic measurements, but to reduce the extinction effect it was cut to a parallelepiped of 1 mm$\times$1 mm$\times$6 mm with the long axis along the [110] direction. The sample was sealed in an aluminum can filled with He gas and set in a closed-cycle helium refrigerator with one of the [110] axes vertical to the scattering plane and was cooled down to 2.0 K. About 20 fundamental satellites have been measured in the $(1\bar{1}0)$ plane at 2 K, and by comparing the intensity of equivalent reflections such as (±0.575 1.425 1.425) with **Q** directions along the [111] and $[\bar{1}11]$, the **Q**-domain distribution is evaluated to be almost equivalent for two directions, and so in the present experimental condition the **Q** domain is considered to populate uniformly in four directions in the cubic crystal. For extinction corrections nuclear reflection has been measured over ten Bragg points.

The temperature dependence of the fundamental satellites was measured for a pair of magnetic reflections at (0.425, 0.425, 0.425) and (0.575, 0.575, 0.575) from 2 K to above the T_N. Figure 7 shows the integrated intensity of both peaks plotted on the same scale as a function of temperature, to-

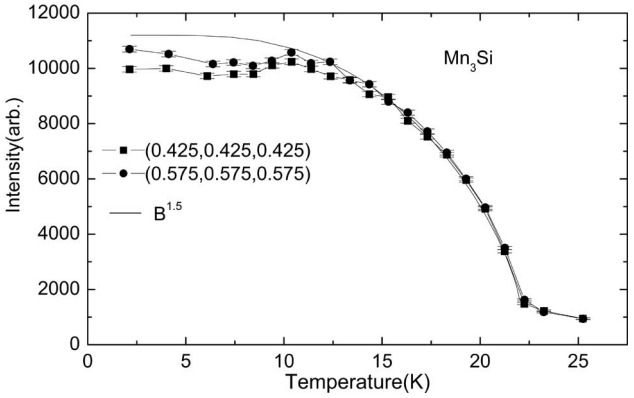

FIG. 7. Integrated peak intensities of a pair of 1**Q** satellites as a function of temperature. A Brillouin curve B of $S=1/2$ with its 1.5th power ($B^{1.5}$ in the figure) is plotted. A deviation from the Brillouin curve is observed apparently below 8 K.

gether with a Brillouin curve for $S=1/2$. In the temperature region from T_N to 10 K the 1.5th power of the Brillouin function ($B^{1.5}$) fits both of the data sets well instead of the usual temperature dependence of the square of magnetization (B^2). This is likely to be a result of a large temperature shift of the propagation vector just below T_N, from which the Bragg peak position shifts as a function of temperature. But below 10 K the integrated intensity goes down from the Brillouin curve extrapolated to the low-temperature region with a maximum drop of about 10% from the calculated curve around 7 K. Since the decrease in intensity occurs at the same temperature for both of the satellites, this suggests a phase transition which may be associated with the disappearance of the 3**Q** harmonic satellites. We considered the possibility of the change of the spin structure from longitudinal to sinusoidal structure as observed in chromium, but in this case only the decrease in the peak intensity without symmetry change was observed. This behavior is anomalous, so we repeated the measurements and confirmed the decrease of the intensity below 10 K. This anomalous temperature variation suggests the interplay between the 1**Q** and 3**Q** harmonics, in which the existence of the 3**Q** harmonics suppresses the amplitude of the fundamental SDW's.

Figure 8 shows the wave vector **Q** as a function of temperature, which was determined by peak fitting using a Gaussian curve for a peak at (0.575, 0.575, 0.575) and the same result was obtained for (0.425, 0.425, 0.425) satellite. In the temperature range from 2 to 8 K, where the 3**Q** harmonics exist, the wave vector keeps almost a constant value of $\mathbf{Q}=0.425\mathbf{G}_{111}$, and from 8 to 10 K the **Q** value decreases to $\mathbf{Q}=0.42\mathbf{G}_{111}$, has a minimum at 10 K, and above 10 K the **Q** value increases linearly with temperature. Just below T_N it rapidly approaches the commensurate value $\mathbf{Q}=1/2\mathbf{G}_{111}$, where double satellite peaks transform to a single peak above T_N.[20] From the present measurement of temperature variation of the **Q** value the detailed behavior around 10 K becomes clear compared to the previous results[6] and it is found that the **Q** value is closely connected with the occurrence of 3**Q** harmonics. In chromium the **Q** vector is a nesting vector connecting a pair of electron and hole Fermi surfaces, so the variation of the **Q** value means some change in the band

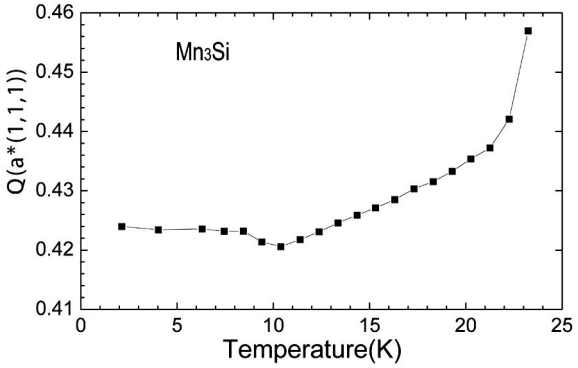

FIG. 8. Temperature dependence of the wave vector **Q** obtained for 1**Q** satellites at (0.575, 0.575, 0. 575) by a Gaussian fitting. Below 8 K it keeps almost a constant value, but after reaching a minimum at 10 K it approaches rapidly to a commensurate value of $(1/2)\mathbf{G}_{111}$ near T_N.

structure. In Mn_3Si the variation of the **Q** value around 8 K may be due to electronic band-structure effects and this is a very interesting phenomenon.

D. Measurements of specific heat and magnetic susceptibility

The specific heat was measured in increasing temperature using a relaxation-type heat-capacity equipment, using a TSZ single-crystal sample in magnetic fields from zero to 6 T. Figure 9 shows the specific heat divided by temperature $C(T)/T$ as a function of temperature, in magnetic fields of zero and 6 T. The large λ-type peak is due to the antiferromagnetic phase transition with T_N of 23 K, and our data for the temperature dependence of specific heat agree well with previous specific heat data measured using polycrystalline samples, except for a sharpening of the peak at the T_N,[5,8] which is probably due to the use of a single-crystal sample. In addition to this peak a very small hump was observed at about 8 K on the shoulder of the magnetic specific heat. The small hump part is shown on an expanded scale in the inset in Fig. 9, which is obtained by subtracting the main λ peak using a smooth curve fitted to data points excluding the tem-

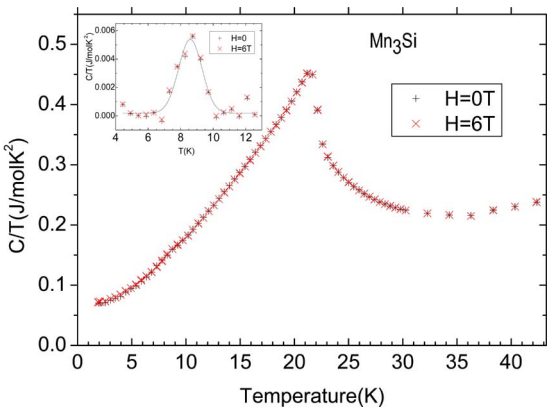

FIG. 9. (Color online) Specific heat divided by temperature (C/T) as a function of temperature at magnetic fields of $H=0$ and 6 T. Expansion of a small peak around 8 K is inserted.

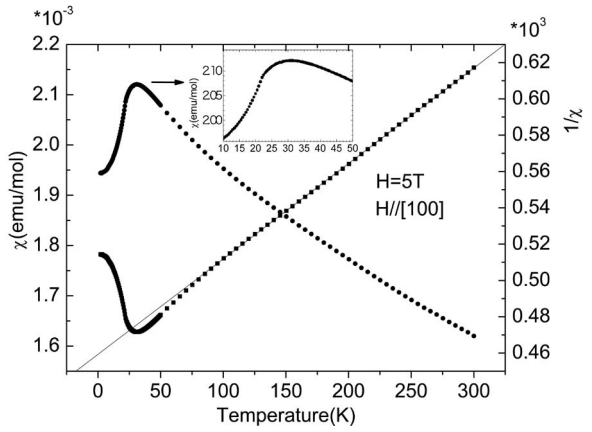

FIG. 10. Magnetic susceptibility and its inverse of Mn_3Si as a function of temperature at a magnetic field of 5 T along the [110] axis. Expansion near T_N is inserted in the figure.

perature region from 6 to 10 K. Evidently the hump shows a clear peak from 7 to 9 K with a maximum at 8.5 K, where the solid line shows a Gaussian curve fitted to the data points. This peak just corresponds to the temperature region where the amplitude of 3**Q** harmonics suddenly decreases and becomes zero. The peak height of this hump is about 2.2% that of the main magnetic peak, a very small specific heat change, so we can ascribe this peak to the disappearance of the 3**Q** harmonics or associated change of the amplitude of the 1**Q** harmonics, since the 3**Q** moment is only 1/40 that of the 1**Q** moment and the change of the 1**Q** moment at 10 K is less than 5%.

Concerning the magnetic field dependence, the data points measured without magnetic field agree quite well with those measured at 6 T within experimental accuracy over the whole temperature range. Especially for the small hump, no change in peak shift and width has been observed, as shown in the inset in Fig. 9. The present result is consistent with the results obtained by Pfleider *et al.*[8,9] who showed that there was no detectable variation in the specific heat by the application of a strong magnetic field up to 14 T. The strong stability of the magnetic state against magnetic fields suggests an incompatibility with the weak itinerant electron magnetism expected for the conventional Fermi liquid. The lack of an observable change on the peak at 8 K in Fig. 9 due to application of strong magnetic fields indicates that 3**Q** harmonics continue to exist over very high magnetic fields and thus the same spin structure is conserved.

The dc magnetic susceptibility was measured with a superconducting quantum interference device (SQUID) magnetometer using single-crystal samples cut from the same TSZ crystal used for the higher-harmonic measurements. Figure 10 shows the temperature variations of the magnetic susceptibility and its inverse for an applied magnetic field of 5 T along the [110] axis. The magnetic susceptibility follows the Curie-Weiss law in the paramagnetic state from which the effective magnetic moment was determined to be $\mu_{eff} = 1.25\mu_B$/Mn. This value is almost consistent with averaged root-mean-square Mn magnetic moments determined by the neutron diffraction in the SDW state. The susceptibility shows a broad maximum around 30 K, and below that it decreases gradually and the curve changes from convex to concave at an inflection point that just corresponds to the T_N determined by neutron diffraction and heat capacity measurements. For other directions such as [100] and [111] the same behaviors of the susceptibility were observed and around 8 K no anomaly has been observed for three directions [100], [110], and [111]. In low fields a rapid decrease of the magnetic susceptibility below 15 K was observed for some directions, but this temperature is higher than the transition temperature of the 3**Q** harmonics observed by neutron diffraction. Therefore what is happening at this temperature below 100 Oe is not understood at present.

III. ANALYSIS OF NEUTRON DIFFRACTION DATA

The presence of the 3**Q** harmonics in Mn_3Si revealed by the present neutron diffraction experiments suggests the possibility of a sinusoidal modulated structure as the spin structure of Mn_3Si rather than a helical modulation. Therefore in the present spin structure analysis we assume a transverse sinusoidal structure propagating along the z axis with spins modulating in the x-z plane, with the magnetic Bragg intensity for the 1**Q** and 3**Q** satellites being given as follows:[21]

$$I(\mathbf{G}_{hkl} \pm \mathbf{Q}) \propto \left(\frac{e^2\gamma}{2mc^2}\right)^2 (1-\varepsilon_x^2)|F(\mathbf{G}_{hkl} \pm \mathbf{Q})|^2. \quad (3)$$

For a fundamental satellite,

$$|F(\mathbf{G}_{hkl} \pm \mathbf{Q})|^2 = |\textstyle\sum_i S_i f_i \exp[i(\mathbf{G}_{hkl} \pm \mathbf{Q}) \cdot \mathbf{r}_i \mp i\phi_i]|^2 \quad (4)$$

and for a 3**Q** satellite

$$|F(\mathbf{G}_{hkl} \pm 3\mathbf{Q})|^2 = |\textstyle\sum_i S_i f_i \exp[i(\mathbf{G}_{hkl} \pm 3\mathbf{Q}) \cdot \mathbf{r}_i \mp i\phi_i]|^2, \quad (5)$$

where $\varepsilon_x (=\sin\theta\cos\varphi)$ is the x component of a unit scattering vector (θ and φ being angles in polar coordinates), $F(hkl)$ the magnetic structure factor, G_{hkl} the reciprocal lattice vector representing Bragg peak (hkl), and S_i, f_i, r_i, and ϕ_i spin values, magnetic form factor, atomic position, and phase factor for site i in a unit cell, respectively.

In Mn_3Si the wave vector of the 3**Q** harmonics is $3\mathbf{Q} = 1.275\mathbf{G}_{111}$, so the vector $\mathbf{G}_{hkl} \pm 3\mathbf{Q}$ in Eq. (3) changes to $\mathbf{G}_{h\pm1,k\pm1,l\pm1} \pm 0.275\mathbf{G}_{111}$. This means a change of the Brillouin zone which includes these 3**Q** satellites, where the magnetic structure factors vary depending on the zone index and are given as follows:

$$F(hkl)^2 = 16f^2S_I^2 \quad \text{for } h,k,l \text{ all odd},$$

$$F(hkl)^2 = 16f^2(S_I - 2S_{II})^2 \quad \text{for } h,k,l \text{ even and } 1/2(h+k+l) \text{ even},$$

$$F(hkl)^2 = 16f^2(S_I + 2S_{II})^2 \quad \text{for } h,k,l \text{ even and } 1/2(h+k+l) \text{ odd}.$$

These structure factors are also valid for fundamental satellites. In the above equation the coupling between spins of

TABLE I. Amplitude of magnetic moments of MnI and MnII for 1**Q** and 3**Q** harmonics for a sinusoidal structure of Mn_3Si.

	μ_{MnI} (μ_B)		μ_{MnII} (μ_B)	
1**Q** harmonics[a]	2.4	±0.2	0.3	±0.2
3**Q** harmonics[b]	0.061	±0.020	0.020	±0.020

[a]T=2 K.
[b]T=5 K.

MnI and MnII is assumed to be antiparallel as determined before.[6]

Under the present experimental conditions the transverse sinusoidal structure has several spin planes which are occupied evenly as described above, so that the $(1-\varepsilon_x^2)$ term in Eq. (3) must be averaged over all possible domains. From the symmetry of the cubic crystal structure shown in Fig. 1 the most probable spin planes with the propagation vector along the [111] axis are the (110) or (112) planes which are mutually perpendicular. Both of the planes have three equivalent planes intersecting with each other on the ⟨111⟩ axis with the mutual angle of 120°. Under the experimental conditions without applied magnetic field and pressure it is reasonable to consider that domains of the spin plane are evenly occupied by three equivalent planes. By averaging over the domains the $(1-\varepsilon_x^2)$ term becomes $\frac{1}{2}(1+\varepsilon_z^2)$, where ε_z is the z component of the unit scattering vector.

Next we must consider the domain distribution of the wave vector **Q** for which there are four equivalent ⟨111⟩ directions. This factor reduces the intensity given in Eq. (3) to 1/4. In this case propagating waves of +**Q** and −**Q** constitute a sinusoidal standing wave, so we do not consider ±**Q** domains. By considering these domain distributions the amplitudes of the MnI and MnII moments were determined. The extinction correction was performed for nuclear peaks,[22] but for magnetic reflections including fundamental and 3**Q** satellites the extinction correction has not been performed because this effect is negligibly small for these magnetic reflections. By using the above formula the maximum amplitudes of 1**Q** and 3**Q** moments were determined from the measured satellites intensity and the results are listed in Table I.

The maximum amplitudes of MnI and MnII for the 1**Q** harmonics determined at 2.0 K are $\mu_{MnI}=2.4\mu_B$ and $\mu_{MnII}=0.30\mu_B$, respectively. These values agree well with the previous ones which are derived for a helical structure,[6] so a factor of $\sqrt{2}$ must be multiplied to compare the maximum amplitude of the sinusoidal structure.

Next the amplitudes of the 3**Q** harmonics determined at 5.0 K are $\mu_{3Q}(\mathrm{MnI})=0.061\mu_B$ and $\mu_{3Q}(\mathrm{MnII})=0.02\mu_B$, respectively, as listed in Table I. The amplitude of the 3**Q** moment is very small compared to the 1**Q** amplitude and 1/40 and 1/15 for MnI and MnII moments, respectively. The former ratio is comparable to the ratio observed in chromium and is considered to be reasonable in 3d metallic systems as the 3**Q** harmonic SDW.

IV. DISCUSSION

In the present experiment we found 3**Q** harmonic SDW's in Mn_3Si at low temperatures, which is a rare case in 3d electron systems except for chromium and its alloys. Higher-harmonic satellites are often observed in rare-earth systems, where large magnetocrystalline anisotropy due to 4f orbital deforms the sinusoidal modulation of the localized magnetic moments. In HoAg and TmAg (cubic CsCl type) a transversal sinusoidal structure accompanies 3**Q** harmonic satellites in the whole temperature region below T_N, where the intensity ratio between 3**Q** and 1**Q** harmonics, I_{3Q}/I_Q, is estimated to be about 1/200 at low temperature.[23] In $ErNi_2B_2C$ (bct) where superconductivity and antiferromagnetism coexist, higher harmonics have fairly large magnetic moments $\mu_{1Q}=9.5\mu_B$, $\mu_{3Q}=2.8\mu_B$, and $\mu_{5Q}=1.5\mu_B$ at low temperature due to a squaring up of the sinusoidal modulated structure with decreasing temperature. In $HoNi_2B_2C$, which is the same system as $ErNi_2B_2C$, no higher harmonic has been observed for a pure spin spiral state, but by a change from spiral to bunched spiral structures due to strong magnetic anisotropy the occurrence of higher harmonics has been identified.[24] And also for cycloyd structures of $DyFe_4Al_8$ and $HoFe_4Al_8$ higher-harmonic satellites have been observed up to seventh order by neutron diffraction.[25] In rare-earth compounds modulated magnetic structures occur mainly from RKKY interactions and the pure sine-wave modulation below T_N tends to square up in general in low temperatures for most sinusoidal modulated structures.

The higher-harmonic satellites observed in Mn_3Si seem completely different from those observed in rare-earth systems because of the very small amplitude of higher harmonics relative to the fundamental ones and because magnetocrystalline anisotropy is almost zero due to its cubic nature. In 3d itinerant electron systems SDW states with incommensurate spin structures reported until now are in most cases confined to spiral structures, such as MnSi,[26] $FeGe_2$,[27] $V_{2-y}O_3$,[3] etc., for which higher-harmonic satellites have not been observed. Chromium is the only example which shows higher-harmonic satellites, whose spin modulation is a transversal sinusoidal wave above the spin-flop transition temperature (112 K) and a longitudinal wave below. Many theories have been developed to the explain SDW state in chromium. Among them Walker[28] suggests from a free-energy analysis that 3**Q** harmonics occur only in linearly polarized waves (transversal sinusoidal and longitudinal) and for circularly polarized waves (helical) the amplitude of 3**Q** harmonics becomes zero, for both wave vector directions of [100] and [111]. Because the crystal symmetry of Mn_3Si is different from that of chromium (O_h point symmetry of MnI is the same as that of chromium), the application of Walker's theory to Mn_3Si is not straightforward. However, his theory seems to be valid to the sinusoidal modulated structure in Mn_3Si.

Figure 11 shows the sinusoidal spin structure of Mn_3Si with the wave vector $\mathbf{Q}=0.425\mathbf{G}_{111}$ along the [111] direction, where the magnetic moment modulates with the phase $\phi_j=0.425\mathbf{G}_{111}\cdot\mathbf{r}_j$ at the position r_j as shown in the figure. The magnetic moments of MnI and MnII couple antiparallel as shown in the figure, where dotted lines show their amplitude modulation. These modulations can be expressed by envelopes for respective Mn moments using the incommensurability $\delta=0.075\mathbf{G}_{111}$ that corresponds to a wave length of $2_\Pi/(0.075\mathbf{G}_{111})=4.4$ unit cells. As shown in Fig. 11 the MnII

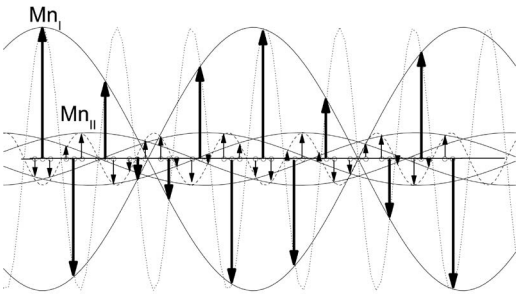

FIG. 11. Transverse sinusoidal spin structure of Mn_3Si determined from 1**Q** harmonic satellites. There are three envelopes of the amplitude corresponding to MnI and MnII moments. The dotted lines show the modulation due to $\mathbf{Q}=0.425\mathbf{G}_{111}$. The scale of MnII moments is expanded against that of MnI to show the modulation clearly.

moment has two envelopes with advanced and retarded phases, corresponding to their positions relative to that of the MnI site along the [111] direction, which arise because the unit cell consists of three fcc manganese lattices with different atomic sites. The presence of MnII moments makes the modulation complicated and smears out the nodes of the MnI envelope, which may reduce or obscure the exchange striction arising from the nodes of the sinusoidal modulation of MnI moments. This is in contrast to the case of chromium, where the exchange striction is large at the node positions.

In chromium it is pointed out that the 2**Q** harmonic satellites arise mainly from the strain-wave distortion due to exchange striction and the contribution from the charge density wave is small.[17] This is a very interesting point in considering the situation in Mn_3Si where strain-wave distortion due to exchange striction is considered to be very small because of the smearing out of the sinusoidal modulation of MnI moment by the addition of MnII modulation. Therefore, if the occurrence of the 2**Q** harmonics is realized as suggested in the present experiment, 2**Q** harmonics will be comprised from mainly CDW's and the strain-wave contribution is suspected to be negligibly small.

It is very interesting to compare the present results with an incommensurate antiferromagnet MnSi which has a cubic unit cell with T_N of 29.5 K. MnSi is believed to be a typical weakly magnetic material with a low ordering temperature and low magnetic moments. The spin structure of MnSi is a helical SDW with a wave vector of $\mathbf{Q}=0.016a^*$ (1,1,1). This state is very near to ferromagnetism, and by applying weak magnetic fields the helical structure changes to a conical structure and becomes a ferromagnet above 6 kOe.[26] The easy change of the magnetic structure by weak magnetic fields suggests that magnetocrystalline anisotropy is very small due to the cubic nature of the structure, and also the helical spin arrangement is sensitive to external magnetic fields compared to a sinusoidal-modulated structure in contrast to the case of Mn_3Si where the magnetic state keeps stiffness against strong magnetic fields as shown by present specific heat and also data by Pfleider *et al.*[8] The magnetic excitations in MnSi exhibit Stoner-excitation-like behaviors at higher energies,[29] resembling that in Mn_3Si, where magnetic excitations persist to higher energy, concentrating around the magnetic zone center. These high-energy magnetic excitations are considered to have close correlation with the stiffness against magnetic field, but in MnSi the magnetic state is sensitive to the external field. These are very contrasting points in comparing two manganese silicides having similar magnetic ordering temperatures.

An energy band calculation performed by an augmented spherical-wave method by Mohn and Supanetz[30] indicates that in Mn_3Si a stable state with a spin spiral structure occurs at a wave vector $\mathbf{Q}=0.43\mathbf{G}_{111}$ whose value agrees quite well with the experimentally determined wave vector, and also a metastable state occurs as an another minimum in the total energy at the commensurate wave vector of $\mathbf{q}=a^*$ (1/2,0,0). Whether or not the same energy minimum is obtainable at the experimentally determined wave vector **Q** by assuming a sinusoidal structure is a very interesting problem. Vlasov *et al.*[31] also calculated the Fermi surface of Mn_3Si and indicated that there is no nesting vector corresponding to the wave vector $\mathbf{Q}=0.425\mathbf{G}_{111}$. Instead they suggest that there are flat portions of the Fermi surface that make the nesting possible with a vector $\mathbf{q}_N=a^*$ (1/2,0,0) which agrees with the wave vector corresponding to the metastable state obtained by Mohn and Supanetz[30] who suggested that in Mn_3Si the nesting induces a SDW instability with the wave vector $\mathbf{q}_N$ in addition to the antiferromagnetic order with $\mathbf{Q}=0.425\mathbf{G}_{111}$. The anomalous behaviors of Mn_3Si observed in the present experiments may be ascribed to the existence of a metastable state at the nesting vector $\mathbf{q}_N$ in addition to the stable antiferromagnetic state with the wave vector **Q**. Further theoretical and experimental studies may provide an advance in understanding SDW's in metallic systems.

In the present work we investigated higher-harmonic SDW's and their effect on the fundamental SDW, from which we discussed the plausible spin structure of Mn_3Si. However, it may be possible to determine the spin structure of linearly or circularly polarized SDW's directly by a method of neutron polarimetry, CRYOPAD (Ref. 32) (cryogenic polarization analysis device). So as a next step such polarized neutron diffraction is very attractive, and also x-ray diffraction will give more detailed information about higher harmonics.

V. CONCLUSION

In conclusion in Mn_3Si the 3**Q** harmonic satellites have been revealed to exist at low temperatures with the amplitude of magnetic moment of about 1/40 that of the fundamental. The 3**Q** harmonic satellites disappear at about 9 K, far below the T_N, with a first-order phase transition. The existence of the 3**Q** harmonics suppresses the amplitude of fundamental harmonics, and associated with this transition the intensity of the fundamental satellite peaks increases above 10 K. From the existence of the 3**Q** harmonics the spin structure was suggested to be a sinusoidal SDW with maximum amplitudes $\mu_{MnI}=2.4\mu_B$ and $\mu_{MnII}=0.3\mu_B$ for MnI and MnII atoms, respectively. Consistent with the previous results, the magnetic field dependence of the specific heat shows stiffness of the magnetic state of Mn_3Si against the strong magnetic field,

and the small specific heat peak at 8.5 K was found to exist even for fields greater than 6 T, which suggests that the 3**Q** harmonics persist to very high magnetic fields, keeping the same spin structure. Finally the 2**Q** harmonics have been observed. However, their confirmation is not perfect, so in the present experiments only the possible existence is pointed out. More careful neutron diffraction and x-ray diffraction are required to clarify higher harmonics and its related problems.

ACKNOWLEDGMENTS

We benefited greatly from conversations with the late Dr. G. Shirane. We would like to thanks Dr. Y. Yamaguchi, Tohoku University, and Dr. M. Kataoka, Iwaki Meisei University, for helpful discussions, and K. Nemoto and T. Miura for technical support. Part of this work was performed under the U.S.-Japan cooperative Neutron Scattering Program.

[1] E. Fawcett, Rev. Mod. Phys. **60**, 209 (1988).
[2] J. Ruvalds, C. T. Rieck, S. Tewari, J. Thoma, and A. Virosztek, Phys. Rev. B **51**, 3797 (1995).
[3] Wei Bao, C. Broholm, S. A. Carter, T. F. Rosenbaum, G. Aeppli, S. F. Trevino, P. Metcalf, J. M. Honig, and J. Spalek, Phys. Rev. Lett. **71**, 766 (1993).
[4] B. Aronson, Acta Chem. Scand. (1947-1973) **14**, 1414 (1960).
[5] G. I. Kalishevich, Yu. A. Vereshagin, and P. V. Gel'd, Sov. Phys. Solid State **16**, 1151 (1974).
[6] S. Tomiyoshi and H. Watanabe, J. Phys. Soc. Jpn. **39**, 295 (1975).
[7] S. A. Werner, A. Arrott, and H. Kendrick, Phys. Rev. **155**, 528 (1967).
[8] C. Pfleiderer, J. Boeuf, and H. v. Löhneysen, Phys. Rev. B **65**, 172404 (2002).
[9] C. Pfleiderer, J. Magn. Magn. Mater. **226-230**, 23 (2001).
[10] M. Doerr, J. Bœuf, C. Pfleiderer, M. Rotter, N. Kozlova, D. Eckert, P. Kerschl, K. Müller, and M. Loewenhaupt, Physica B **346-347**, 137 (2004).
[11] S. Fujii, S. Ishida, and S. Asano, J. Phys. Soc. Jpn. **64**, 185 (1995).
[12] S. Tomiyoshi, Y. Yamaguchi, M. Ohashi, E. R. Cowley, and G. Shirane, Phys. Rev. B **36**, 2181 (1987).
[13] S. Tomiyoshi, Y. Yamaguchi, M. Ohashi, E. R. Cowley, and G. Shirane, J. Magn. Magn. Mater. **70**, 236 (1987).
[14] Y. Tsunoda, M. Mori, N. Kunitomi, Y. Teraoka, and J. Kanamori, Solid State Commun. **14**, 287 (1974).
[15] R. Pynn, W. Press, and S. M. Shapiro, Phys. Rev. B **13**, 295 (1976).
[16] J. P. Hill, G. Helgesen, and D. Gibbs, Phys. Rev. B **51**, 10336 (1995).
[17] K. Hirai, J. Phys. Soc. Jpn. **66**, 560 (1997).
[18] A. B. Gokhale and R. Abbaschlan, Bull. Alloy Phase Diagrams **11**, 468 (1990).
[19] G. H. Lander, P. J. Brown, and J. B. Forsyth, Proc. Phys. Soc. London **91**, 332 (1967).
[20] Y. Yamaguchi, T. R. Thurston, H. Miki, and S. Tomiyoshi, Physica B **213&214**, 363 (1995).
[21] *Introduction to Physical Techniques in Molecular Magnetism*, edited by F. Palacio, E. Ressouche, and J. Schweizer (Yesa, 1999), Servicio de Publicaciones de la Universidad de Zaragoza, Pt. I, p. 191; S. W. Lovesey, *Theory of Neutron Scattering from Condensed Matter* (Clarendon Press, Oxford, 1984), Vol. 2.
[22] W. H. Zachariasen, Acta Crystallogr. **23**, 558 (1967).
[23] P. Morin, D. Schmitt, and C. Vettier, J. Phys. (Paris) **46**, 39 (1985).
[24] J. W. Lynn, S. Skanthakumar, Q. Huang, S. K. Sinha, Z. Hossain, L. C. Guputa, R. Nagarajan, and C. Godart, Phys. Rev. B **55**, 6584 (1997).
[25] J. A. Paixao, M. R. Silva, S. Aa. Sorensen, B. Lebech, G. H. Lander, P. J. Brown, S. Langridge, E. Talik, and A. P. Goncalves, Phys. Rev. B **61**, 6176 (2000).
[26] Y. Ishikawa, K. Tajima, D. Bloch, and M. Roth, Solid State Commun. **19**, 525 (1976).
[27] L. M. Corliss, J. M. Hastings, W. Kunnmann, R. Thomas, J. Zhuang, R. Butera, and D. Mukamel, Phys. Rev. B **31**, 4337 (1985), C. P. Adams, T. E. Mason, E. Fawcett, A. Z. Menshikov, C. D. Frost, J. B. Forsyth, T. G. Perring, and T. M. Holden, J. Phys.: Condens. Matter **12**, 8487 (2000).
[28] M. B. Walker, Phys. Rev. B **22**, 1338 (1980).
[29] Y. Ishikawa, J. Magn. Magn. Mater. **54-57**, 1121 (1986).
[30] P. Mohn and E. Supanetz, Philos. Mag. B **78**, 629 (1998).
[31] A. V. Vlasov, E. T. Kulatov, and A. A. Povzner, Sov. Phys. Lebedev. Inst. Rep. **12**, 5 (1990).
[32] P. J. Brown, V. Nunez, F. Tasset, J. B. Forsyth, and P. Radhakrishna, J. Phys.: Condens. Matter **2**, 9409 (1990).